International Journal of Thermal Sciences 48 (2009) 1060–1067

Contents lists available at ScienceDirect

International Journal of Thermal Sciences

www.elsevier.com/locate/ijts

Developing a method for coupling branch modal models

P.O. Laffay *, O. Quéméner, A. Neveu

Laboratoire de Mécanique et d'Energétique d'Evry, 40 rue du Pelvoux, CE1455 Courcouronnes, 91020 Evry Cédex, France

ARTICLE INFO

Article history:
Received 12 October 2007
Received in revised form 5 November 2008
Accepted 5 November 2008
Available online 2 December 2008

Keywords:
Reduction
Modal analysis
Eigenvalue problem
Branch modes
State equations
Thermal contact resistance
Domain decomposition methods

ABSTRACT

An original method is proposed to reduce diffusion problem characterized by a thermal contact resistance and non-linear boundary conditions. The method use a substructuring technique in which a branch modal basis is obtained for each subdomain. The amalgam reduction method for each basis leads to a global reduced model. A specific flux jump functional allows to optimize reduction. The numerical test case is an electronic component coupled with a radiator and which follows a thermal regulation. For this case a numerical study is made in order to observe the influence of the flux jump functional. Comparison between the detailed model and the reduced one with optimal parameters gives a gain in computation time of 82 for the same precision.

1. Introduction

Among the different methods allowing to reduce a thermal conduction problem [3,5], the modal method [16–18] linked to the amalgam reduction [13], showed its efficacity. The modal method has been extended to non-linear or time-dependent parameters cases by using a particular modal basis called the branch basis [12]. Recently an adaptation of the amalgam reduction has been proposed for the branch modes [14]. The aim of this method is to be as general as possible. However two kinds of cases could not be solved by the branch method: At first in the actual formulation it is not possible to take an internal thermal contact resistance into account. Secondly, in case of very complex mesh corresponding to a realistically complex physical problem, the branch basis computation is difficult because of computer memory limitation. In order to overcome those obstacles, the substructuring technique seems to be well adapted. This technique has been widely used for mechanical problems [2], and corresponds to the following steps:

- the domain is separated in several adjacent subdomains;
- for each subdomain, a set of eigenmodes is computed;
- the different reduced states-equations corresponding to the several subdomains are linked to each other by internal boundary conditions and solved;
- the reconstitution of the thermal field can then be carried out.

There are few papers concerning thermal reduced model coupling. Flament et al. [7] proposed a method called modal synthesis, limited to perfect thermal contacts between the subdomains. The modal synthesis technique is only used for the eigenmodes determination. Specific coupling modes are added to each local basis yielding a new basis in the full domain. The modal reduction procedure is then classical. Another method is proposed by El Biyaali et al. [6]. Their approach is numerical and instead of computing coupling modes, a new diagonalization of the system is performed. Menezo et al. [11] proposed a substructuring method for radiative conditions, which takes into account internal boundaries between non-adjacent subdomains and considers non-linear coupling conditions on those internal boundaries.

However all of these works use classical eigenmodes (Fourier, Neumann or Dirichlet modes defined by Eq. (9) and respective boundary conditions) which are not rigorously adapted to non-linear problems, and which lead to difficulties for the subdomains coupling step. An extension of classical modes is made by the branch eigenvectors, allowing consideration of non-linear problems.

This paper presents the branch modal substructuring theory and stresses on the necessity to add a new functional in the thermal problem. This functional minimizes the numerical flux jump on an internal boundary and increases the reduced model efficacy. An analysis of the influence of the flux jump penalization coefficient is performed, and we propose a technique allowing a blind choice of this parameter. A test case is then treated: this concerns an electronic component provided with thermal regulation. Precise results are obtained in a very small CPU time, showing the interest of the method.

* Corresponding author. Tel.: +33 1 69 47 79 38; fax: +33 1 69 47 79 47.
E-mail address: laffay@crans.org (P.O. Laffay).

1290-0729/$ – see front matter
doi:10.1016/j.ijthermalsci.2008.11.002

Nomenclature

c	volumetric heat capacity	$\mathrm{J\,K^{-1}\,m^{-3}}$
f	arbitrary function	
h	convective coefficient	$\mathrm{W\,m^{-2}\,K^{-1}}$
k	thermal conductivity	$\mathrm{W\,m^{-1}\,K^{-1}}$
M	spatial parameter	
N	detailed model dimension	
$\widetilde{N}_0$	branch basis dimension	
$\widetilde{N}_1$	reduced branch basis dimension	
$\underline{n}$	unit normal exterior vector	
T	temperature	K
t	time	s
v	test function	
V	branch eigenvector	K
$\mathcal{V}$	structured branch eigenvector	K
x	state vector	
z	eigenvalue	$\mathrm{s^{-1}}$

Greek symbols

$\Omega, \partial\Omega$	domain and boundaries
Γ	physical interface
α	amalgam coefficient
β	flux jump penalization coefficient
γ	maximum of the state vector evolution norm divided by the time increment
τ	eigenmode time constant (s)
ζ	Steklov number ($\mathrm{kg\,s^{-2}\,K^{-1}}$)
π	volumic source of energy ($\mathrm{W\,m^{-3}}$)

Abbreviation

BRM	Branch Reduced Model
TCR	Thermal Contact Resistance ($\mathrm{m^2\,K\,W^{-1}}$)

Superscripts

(j)	relative to domain $\Omega^{(j)}$
ext	exterior
amb	ambient
$\widetilde{V}$	reduced branch eigenvector
$\widetilde{\mathcal{V}}$	reduced structured branch eigenvector

2. Branch modal substructuring theory

2.1. Description of the physical problem

Let Ω be a physical domain partitioned in two parts $\Omega^{(1)}$ and $\Omega^{(2)}$.

Let the unit normal exterior vectors be $\underline{n}$, $\underline{n}^{(1)}$, $\underline{n}^{(2)}$ for domains Ω, $\Omega^{(1)}$, $\Omega^{(2)}$, respectively, and $\partial\Omega$, $\partial\Omega^{(1)}$, $\partial\Omega^{(2)}$ the boundaries of domains Ω, $\Omega^{(1)}$ and $\Omega^{(2)}$, respectively. $\Gamma^{(12)}$ is the physical interface between $\Omega^{(1)}$ and $\Omega^{(2)}$, modelized by a thermal contact resistance [8].

The jump on $\Gamma^{(12)}$ from $\Omega^{(1)}$ to $\Omega^{(2)}$ for any function f is defined by:

$$\forall M \in \Gamma^{(12)} \quad \left[\!\left[f(M) \right]\!\right]_{\Gamma^{(12)}} \equiv f^{(2)}(M) - f^{(1)}(M) \tag{1}$$

In Eq. (1), $f^{(j)}(M)$ is the value of f in $\Omega^{(j)}$ at point M. It is important to notice that f is double valuated for all point M in $\Gamma^{(12)}$.

Equations of the physical problem (conductivities $k^{(j)}$ and capacities $c^{(j)}$ are only function of space) are:

$$j \in \{1,2\},\ \forall M \in \Omega^{(j)},\ \forall t > 0$$
$$c^{(j)} \frac{\partial T^{(j)}}{\partial t} = \underline{\nabla}\left(k^{(j)} \underline{\nabla}\left(T^{(j)}\right)\right) + \pi^{(j)} \tag{2}$$
$$j \in \{1,2\},\ \forall M \in \partial\Omega^{(j)} \setminus \Gamma^{(12)},\ \forall t > 0$$
$$k^{(j)} \underline{\nabla}\left(T^{(j)}\right) \bullet \underline{n}^{(j)} = h\left(T_{\mathrm{ext}} - T^{(j)}\right) \tag{3}$$
$$\forall M \in \Gamma^{(12)},\ \forall t > 0$$
$$-k^{(1)} \underline{\nabla}\left(T^{(1)}\right) \bullet \underline{n}^{(1)} = -\left(-k^{(2)} \underline{\nabla}\left(T^{(2)}\right) \bullet \underline{n}^{(2)}\right) \tag{4}$$
$$\forall M \in \Gamma^{(12)},\ \forall t > 0$$
$$-k^{(1)} \underline{\nabla}\left(T^{(1)}\right) \bullet \underline{n}^{(1)} = \frac{T^{(1)} - T^{(2)}}{TCR} \tag{5}$$
$$j \in \{1,2\},\ t = 0,\ \forall M \in \Omega^{(j)}$$
$$T^{(j)} = T^{(j0)} \tag{6}$$

Eqs. (4) and (5) express the two conditions of thermal contact resistance: flux continuity and linear dependence between flux and temperature jump. *TCR* is the thermal contact resistance in $\mathrm{m^2\,K\,W^{-1}}$.

2.2. Variational formulation

The weak formulation of Eqs. (2)–(5) is similar to the classical formulation, excepting a new term which takes into account the temperature jump across the interface:

$$\mathcal{C}(\dot{T}, v) = -\left(\mathcal{K}(T, v) + \mathcal{B}(T, v) + \mathcal{J}^{T}_{\Gamma^{(12)}}(T, v)\right) + \mathcal{A}(v) \tag{7}$$

where

$$\begin{cases} \mathcal{C}(f, v) = \displaystyle\iint_{\Omega} cf\, v \,\mathrm{d}\Omega \\ \mathcal{K}(f, v) = \displaystyle\iint_{\Omega} k \underline{\nabla}(v) \bullet \underline{\nabla}(f) \,\mathrm{d}\Omega \\ \mathcal{B}(f, v) = \displaystyle\int_{\partial\Omega} vhf \,\mathrm{d}(\partial\Omega) \\ \mathcal{J}^{T}_{\Gamma^{(12)}}(f, v) = \displaystyle\int_{\Gamma^{(12)}} \frac{\left[\!\left[v \right]\!\right]_{\Gamma^{(12)}} \left[\!\left[f \right]\!\right]_{\Gamma^{(12)}}}{TCR} \,\mathrm{d}\Gamma^{(12)} \\ \mathcal{A}(v) = \displaystyle\int_{\partial\Omega} vhT_{\mathrm{ext}} \,\mathrm{d}(\partial\Omega) + \iint_{\Omega} v\pi \,\mathrm{d}\Omega \end{cases} \tag{8}$$

Temperature field in $\Omega^{(j)}$ is defined in the Hilbert space [9] $H^1(\Omega^{(j)})$ so temperature field in Ω is defined in $H^1(\Omega, \Gamma^{(12)}) \equiv H^1(\Omega^{(1)}) \oplus H^1(\Omega^{(2)})$.

The choice of test functions is then obvious, as soon as we use internal approximation, v are functions of $H^1(\Omega, \Gamma^{(12)})$. Notice that functions of $H^1(\Omega, \Gamma^{(12)})$ are double valuated on $\Gamma^{(12)}$.

2.3. Modal formulation for substructured model

2.3.1. The Branch eigenvalues problem

Branch modes of $\Omega^{(j)}$ define a basis for $H^1(\Omega^{(j)})$ [14]. As branch modes are defined on $\Omega^{(1)}$ or $\Omega^{(2)}$ and test functions v are defined on Ω, a new vector basis is defined from branch modes bases on $\Omega^{(1)}$ and $\Omega^{(2)}$.

Branch modes on $\Omega^{(j)}$ are solutions of the eigenproblem defined by the following equations:

$$j = 1, 2,\ \forall M \in \Omega^{(j)}$$
$$\underline{\nabla}\left(k^{(j)} \underline{\nabla} V_i^{(j)}\right) = z_i^{(j)} c^{(j)} V_i^{(j)} \tag{9}$$

$j = 1, 2,\ \forall M \in \partial\Omega^{(j)}$

$$k^{(j)}\underline{\nabla}V_i^{(j)} \bullet \underline{n}^{(j)} = -z_i^{(j)}\zeta^{(j)}V_i^{(j)} \tag{10}$$

$V_i^{(j)}$ is the i-order branch eigenvector, $z_i^{(j)}$ is the eigenvalue of $V_i^{(j)}$. $\zeta^{(j)}$ is the Steklov function, which ensures the dimensional integrity. Choice of $\zeta^{(j)}$ and branch modes properties are detailed in [14].

A new basis for $H^1(\Omega, \Gamma^{(12)})$ named structured branch mode basis $\{z_{n_i^j}, \mathcal{V}_{n_i^j}\}$ where $\mathcal{V}_{n_i^j}$ is the n-order structured branch eigenvector equal to the $V_i^{(j)}$ branch eigenvector of $\Omega^{(j)}$ extended by 0 on $\Omega \setminus \Omega^{(j)}$. Since local branch modes are not equal to 0 on $\Gamma^{(12)}$, prolongation by 0 implies a discontinuity appearance on $\Gamma^{(12)}$.

Temperature field can be decomposed on the structured branch modes basis:

$$\forall t,\ \forall M \in \Omega \quad T = \sum_{n=1}^{\infty} x_{n_i^j}(t)\mathcal{V}_{n_i^j} \tag{11}$$

Each $x_{n_i^j}(t)$ coefficient is the time dependent excitation state of $\mathcal{V}_{n_i^j}$.

The spatial discretization by the finite element method leads to a finite number of eigenmodes equal to the degree of freedom $N^{(j)}$ of the mesh. Practically, during the eigenmodes computation step, a Marshall truncature [10,14] is made, i.e. the modes characterized by the largest eigenvalue are not computed, $\widetilde{N}_0^{(j)}$ eigenmodes are then obtained.

2.3.2. The amalgam modal reduction

An advantage of a modal basis is its ability to be reduced.

In this study, the reduction of each local basis $\{z_i^{(j)}, V_i^{(j)}\}$ yields a new basis $\{\tilde{z}_i^{(j)}, \widetilde{V}_i^{(j)}\}$ characterized by a dimension $\widetilde{N}_1^{(j)} \ll \widetilde{N}_0^{(j)}$. As previously a reduced structured basis $\{\tilde{z}_{n_i^j}, \widetilde{\mathcal{V}}_{n_i^j}\}$ is obtained from each local reduced basis $\{\tilde{z}_i^{(j)}, \widetilde{V}_i^{(j)}\}$. The complete temperature field is then decomposed as:

$$\forall t,\ \forall M \in \Omega \quad T \approx \widetilde{T} = \sum_{n=1}^{\widetilde{N}_1^{(1)}+\widetilde{N}_1^{(2)}} \tilde{x}_{n_i^j}(t)\widetilde{\mathcal{V}}_{n_i^j} \tag{12}$$

The amalgam reduction [13,14] (for each domain $\Omega^{(1)}$ and $\Omega^{(2)}$) consists in splitting eigenvectors $V_i^{(j)}$ of the branch basis into $\widetilde{N}_1^{(j)}$ subspaces. In each subspace a linear combinaison is performed in order to provide $\widetilde{N}_1^{(j)}$ amalgamated eigenvectors $\widetilde{V}_i^{(j)}$. The amalgam modal basis is then orthogonal.

Coefficient in the linear combination are linked to a physical linear test case. For the substructuring technique, the choice of the test case is delicate, because each subdomain is considered as independant, and the most representative case in comparison with the real physical coupled problem has to be chosen. Section 3.3.2 presents the different used test case.

2.3.3. State equation

From the reduced basis and considering Eq. (12), the problem is to determine the state coefficient. In order to obtain the time-state differential equation, the weak formulation of the physical problem is used (Eq. (8)), the test functions v being the reduced structured branch eigenvectors:

$$\sum_{n=1}^{\widetilde{N}_1^{(1)}+\widetilde{N}_1^{(2)}} \mathcal{C}(\widetilde{\mathcal{V}}_{n_i^j}, \widetilde{\mathcal{V}}_{k_i^j})\dot{\tilde{x}}_{n_i^j} = -\sum_{n=1}^{\widetilde{N}_1^{(1)}+\widetilde{N}_1^{(2)}} \big(\mathcal{K}(\widetilde{\mathcal{V}}_{n_i^j}, \widetilde{\mathcal{V}}_{k_i^j}) + \mathcal{B}(\widetilde{\mathcal{V}}_{n_i^j}, \widetilde{\mathcal{V}}_{k_i^j}) + \mathcal{J}^T_{\Gamma^{(12)}}(\widetilde{\mathcal{V}}_{n_i^j}, \widetilde{\mathcal{V}}_{k_i^j})\big)\tilde{x}_{n_i^j} + \mathcal{A}(\widetilde{\mathcal{V}}_{k_i^j}) \tag{13}$$

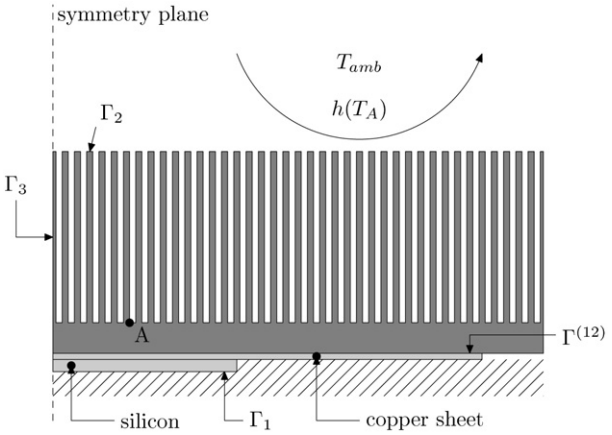

Fig. 1. Physical model.

2.3.4. Flux jump penalization

Due to modal reduction, there is an error on temperature field and this error induces a flux jump at the interface, moreover it is not possible to enforce exactly flux continuity across $\Gamma^{(12)}$. However it is possible to decrease flux jump.

To do so, a new functional is introduced as in discontinuous Galerkin methods [4]. This functional has to present these essential properties: bi-linearity, symmetry and positivity. The functional should also be simple to write and should not increase computation time. Among all the functionals that could be used [4], the following one has been chosen:

$$\mathcal{J}^{\Phi}_{\Gamma^{(12)}}(f, v) = \beta \int_{\Gamma^{(12)}} \left[\!\left[k\underline{\nabla}(f) \bullet \underline{n}^{(12)}\right]\!\right]_{\Gamma^{(12)}} \left[\!\left[k\underline{\nabla}(v) \bullet \underline{n}^{(12)}\right]\!\right]_{\Gamma^{(12)}} \tag{14}$$

The numerical parameter β allows to ensure the dimensional homogeneity and to balance this term according to the others terms of the state equation (13):

$$\sum_{n=1}^{\widetilde{N}_1^{(1)}+\widetilde{N}_1^{(2)}} \mathcal{C}(\widetilde{\mathcal{V}}_{n_i^j}, \widetilde{\mathcal{V}}_{k_i^j})\dot{\tilde{x}}_{n_i^j} = -\sum_{n=1}^{\widetilde{N}_1^{(1)}+\widetilde{N}_1^{(2)}} \big(\mathcal{K}(\widetilde{\mathcal{V}}_{n_i^j}, \widetilde{\mathcal{V}}_{k_i^j}) + \mathcal{B}(\widetilde{\mathcal{V}}_{n_i^j}, \widetilde{\mathcal{V}}_{k_i^j}) + \mathcal{J}^T_{\Gamma^{(12)}}(\widetilde{\mathcal{V}}_{n_i^j}, \widetilde{\mathcal{V}}_{k_i^j}) + \mathcal{J}^{\Phi}_{\Gamma^{(12)}}(\widetilde{\mathcal{V}}_{n_i^j}, \widetilde{\mathcal{V}}_{k_i^j})\big)\tilde{x}_{n_i^j} + \mathcal{A}(\widetilde{\mathcal{V}}_{k_i^j}) \tag{15}$$

3. Application

3.1. The physical problem

We consider a microprocessor, described in 2D geometry (Fig. 1). This electronic component is made up of:

- a silicon ship placed on a copper sheet. Joule effect in the silicon induces a volumic thermal power source π (subdomain 1),
- an aluminium radiator composed of longitudinal fins (subdomain 2).

Physical characteristics of these materials are precised on Table 1. Between both pieces, the thermal contact resistance (*TCR*) cannot be neglected, and leads to a temperature break at the interface. In order to minimize this temperature jump, a thermal interface material is set down at the internal boundary, leading to a $TCR = 25 \times 10^{-6}\ \mathrm{m^2\,K\,W^{-1}}$ [8]. The thermal regulation is controlled by a double speed fan, activated by a thermal sensor placed

Table 1
Materials properties.

	k (W m^{-1} K^{-1})	c (J m^{-3} K^{-1})	π (W m^{-3})
Silicon	145	1 514 500	3.4×10^7
Copper	380	3 363 000	0
Aluminium	216	2 340 000	0

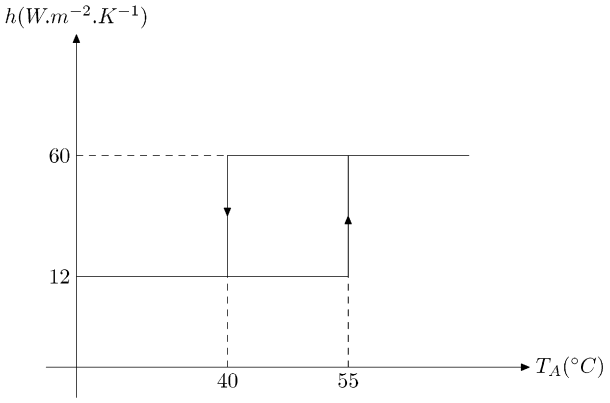

Fig. 2. Convection coefficient evolution.

on the radiator (point A on Fig. 1), leading the convection coefficient follow to an hysteresis (Fig. 2). Ambient temperature is $T_{\text{amb}} = 20\,°\text{C}$.

Γ_1 is the adiabatic boundary of the processor (silicon + copper sheet), $\Gamma^{(12)}$ is the interface between the processor and the radiator, Γ_2 is the radiator convective boundary. The virtual boundary Γ_3 (symmetry plane) is introduced to simplify computation.

The problem equations are:

$$j \in \{1,2\},\ \forall M \in \Omega_j,\ \forall t > 0$$

$$c^{(j)} \frac{\partial T^{(j)}}{\partial t} = k^{(j)} \Delta T^{(j)} + \pi^{(j)} \tag{16}$$

$$j \in \{1,2\},\ \forall M \in \Gamma_1 \cup \Gamma_3,\ \forall t > 0$$

$$\underline{\nabla} T^{(j)} \bullet \underline{n}^{(j)} = 0 \tag{17}$$

$$\forall M \in \Gamma_2,\ \forall t > 0$$

$$-k^{(2)} \underline{\nabla} T^{(2)} \bullet \underline{n}^{(2)} = h(T_A)\left(T^{(2)} - T_{\text{amb}}\right) \tag{18}$$

$$\forall M \in \Gamma^{(12)},\ \forall t > 0$$

$$-k^{(1)} \underline{\nabla} T^{(1)} \bullet \underline{n}^{(1)} = k^{(2)} \underline{\nabla} T^{(2)} \bullet \underline{n}^{(2)} = \frac{T_1 - T_2}{TRC} \tag{19}$$

$$j \in \{1,2\},\ \forall M \in \Omega^{(j)}$$

$$t = 0, \qquad T^{(j)} = T_{\text{amb}} \tag{20}$$

3.2. Numerical resolution of the detailed model

In order to have a reference case, the thermal evolution of the microprocessor is computed by classical finite elements method with linear shape functions (triangle P^1). The temporal discretization scheme is first order implicit, with a variable computation time step. Matrices are described on sparse form, and equations are solved by diagonal preconditioned conjugate gradient method. All simulations are done for an evolution in time from 0 to 1000 s.

After a complete sensitivity analysis, we use as reference a finite element model (A) with 10 472 nodes (1911 nodes for the processor and 8561 for the radiator). Time step determination criterion is the maximum temperature difference between two time steps which has to be less than 0.002 K. The convergence parameter for the matricial solver is chosen equal to 10^{-12}. Computation time is then equal to 48 673 s. Fig. 3 presents the extreme temperatures temporal evolution (model A) while Fig. 4 corresponds to the thermal field at $t = 800$ s (model A). The temperature jump at the interface clearly appears.

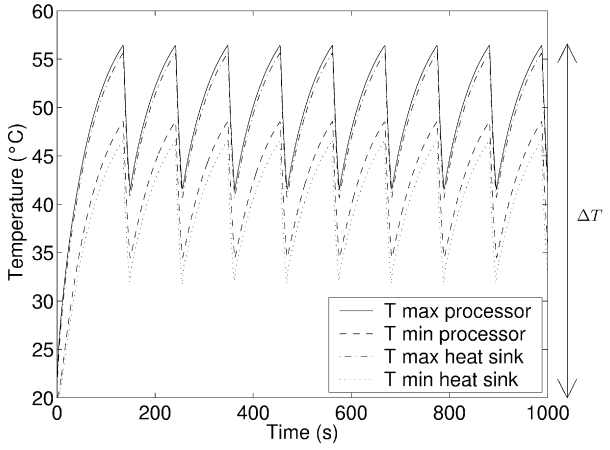

Fig. 3. Extreme temperatures temporal evolution.

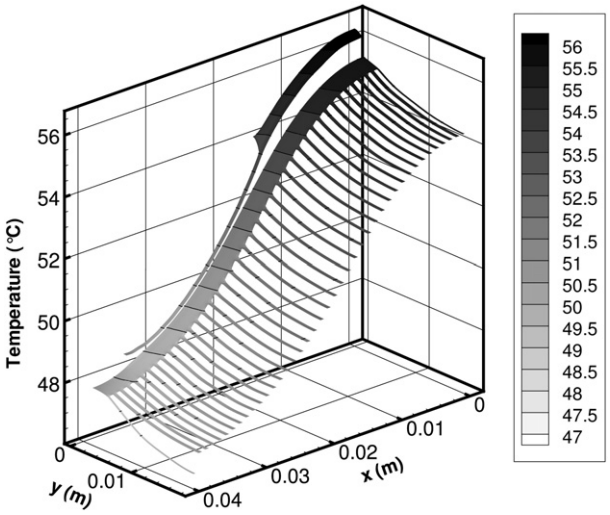

Fig. 4. Thermal field at $t = 800$ s.

In order to compare computation time between a finite element model and a modal reduced model, we looked for a finite element model B for which computation time is not extensive and the maximum error $\epsilon_{AB,\max}$ between model B and model A is less than 1% of the full range temperature evolution ΔT, with:

$$\epsilon_{AB,\max} = \max_t\left(\max_\Omega\left(\text{abs}(T_B - T_A)\right)\right) \tag{21}$$

Model B mesh is equal to model A mesh, but the maximum temperature difference between two time steps is 0.007 K and the convergence parameter for the matricial solver is equal to 10^{-8}. With those choices, the computation time of model B is equal to 16 408 s.

3.3. The reduced model

3.3.1. Eigenproblem

The eigenproblem linked to the precedent physical problem is defined by Eqs. (9)–(10). For both subdomains the respective c and k parameters correspond to the constant physical values. Concerning the Steklov parameter, the classical rules defined in [14] are followed:

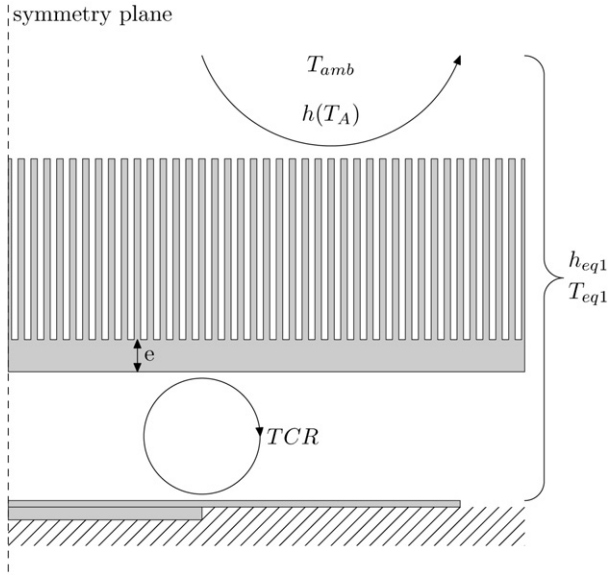

Fig. 5. Choice of the test cases internal boundary condition for processor.

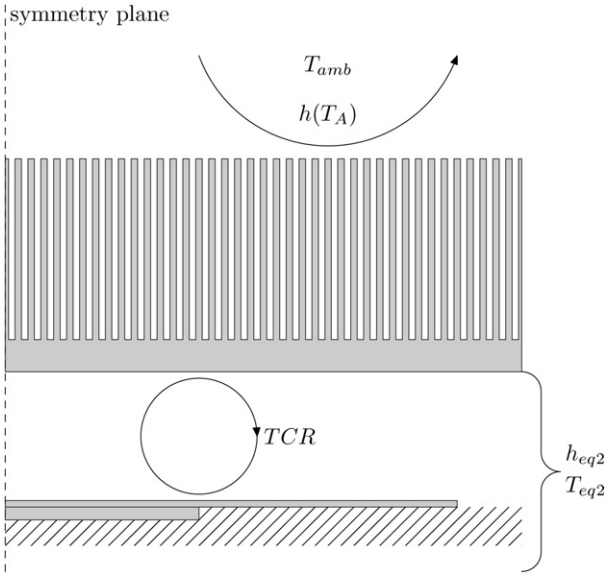

Fig. 6. Choice of the test cases internal boundary condition for radiator.

- $\zeta^{(j)} = 0$ for adiabatic boundaries,
- $\zeta^{(j)} = c^{(j)} \int_{\Omega^{(j)}} \mathrm{d}\Omega^{(j)} / \int_{\partial\Omega^{(j)}} \mathrm{d}(\partial\Omega^{(j)})$ in the other cases.

Eqs. (9)–(10) are discretized by finite elements on model *A* mesh and provide a generalized matricial eigenproblem. This eigenproblem is solved by ARPACK code [1,19] and gives:

- $\widetilde{N}_0^{(1)} = 1750$ eigenmodes for the processor with a computation time of 53 s,
- $\widetilde{N}_0^{(2)} = 5000$ eigenmodes for the radiator with a computation time of 891 s.

3.3.2. Amalgam reduction

For the substructuring technique, the choice of the test case is delicate, because for each subdomain considered as independent, the most representative case in comparison with the real physical coupled problem has to be chosen.

In the considered application, the processor configuration is classical. As shown in Fig. 5, an equivalent convective coefficient for the boundary $\Gamma^{(12)}$ can be estimated by taking into account all the thermal resistance between the boundary and the ambient environment (for a maximum convective coefficient equal to 60 $\mathrm{W\,m^{-2}\,K^{-1}}$):

$$h_{\mathrm{eq1}} = \frac{1}{TCR + \frac{e}{k} + \frac{S_{\Gamma_2}}{S_{\Gamma_3}}\frac{1}{h}} \approx 1000\ \mathrm{W\,m^{-2}\,K^{-1}}$$

$$T_{\mathrm{eq1}} = T_{\mathrm{amb}} \tag{22}$$

The test case corresponding to the processor is then defined by the following equations:

$$\forall M \in \Omega^{(1)},\ \forall t > 0$$

$$c^{(1)} \frac{\partial T^{(1)}}{\partial t} = k^{(1)} \Delta T^{(1)} + \pi^{(1)} \tag{23}$$

$$\forall M \in \Gamma_1 \cup \Gamma_3,\ \forall t > 0$$

$$\underline{\nabla} T^{(1)} \bullet \underline{n}^{(1)} = 0 \tag{24}$$

$$\forall M \in \Gamma^{(12)},\ \forall t > 0$$

$$-k^{(1)} \underline{\nabla} T^{(1)} \bullet \underline{n}^{(1)} = h_{\mathrm{eq1}} \left(T^{(1)} - T_{\mathrm{eq1}}\right) \tag{25}$$

Concerning the radiator, the problem is more delicate, because of the important voluminal thermal power dissipation in the processor and because of the adiabatic condition for the boundary Γ_1. By default, used values are:

$$h_{\mathrm{eq2}} = h_{\mathrm{eq1}}, \qquad T_{\mathrm{eq2}} = \frac{T_{\max} + T_0}{2} = 40\,^{\circ}\mathrm{C} \tag{26}$$

where $T_{\max}$ corresponds to the processor maximum temperature during the simulation. The test case (Fig. 6) corresponding to the radiator is then:

$$\forall M \in \Omega^{(2)},\ \forall t > 0$$

$$c^{(2)} \frac{\partial T^{(2)}}{\partial t} = k^{(2)} \Delta T^{(2)} \tag{27}$$

$$\forall M \in \Gamma_2,\ \forall t > 0$$

$$-k^{(2)} \underline{\nabla} T^{(2)} \bullet \underline{n}^{(2)} = h_{\mathrm{amb}} \left(T^{(2)} - T_{\mathrm{amb}}\right) \tag{28}$$

$$\forall M \in \Gamma^{(12)},\ \forall t > 0$$

$$-k^{(2)} \underline{\nabla} T^{(2)} \bullet \underline{n}^{(2)} = h_{\mathrm{eq2}} \left(T^{(2)} - T_{\mathrm{eq2}}\right) \tag{29}$$

$$\forall M \in \Gamma_3,\ \forall t > 0$$

$$\underline{\nabla} T^{(2)} \bullet \underline{n}^{(2)} = 0 \tag{30}$$

3.3.3. Resolution of the reduced model

From the obtained amalgam modal basis, states can be computed as specified in Eq. (13). At the opposite of the detailed model, as matrices are small but full, a direct resolution algorithm is used: the LDLt method. The temperature field evolution can be built and compared with the results computed by the finite element model *A*.

3.4. Results

With the obtained branch basis $\{z_i^{(1)}, V_i^{(1)}\}$ and $\{z_i^{(2)}, V_i^{(2)}\}$, all the computation steps (amalgam reduction, state equation resolution, temperature building) are made for a large range of the numerical parameters specified above, i.e.:

- internal boundary conditions for the amalgam test cases (h_{eq1}, T_{eq1}, h_{eq2} and T_{eq2}),
- order of reduction by domain $\widetilde{N}$,
- flux jump penalization function parameter β.

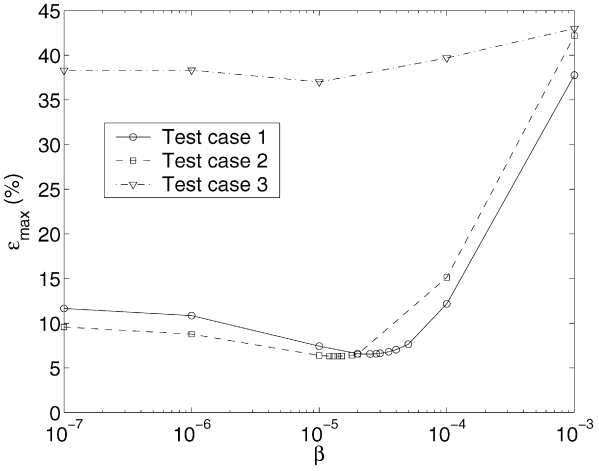

Fig. 7. Maximum error for a reduction order by domain equal to 10.

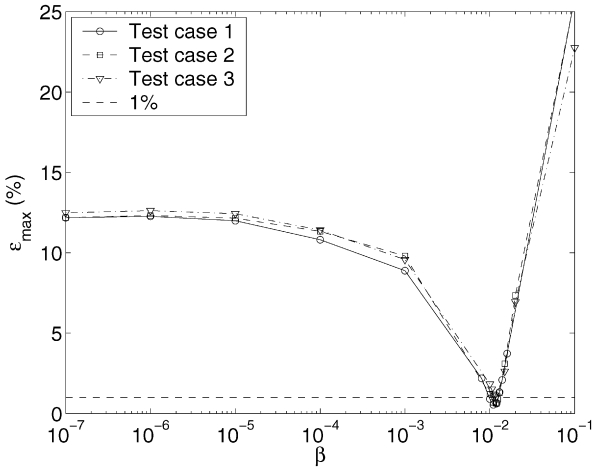

Fig. 8. Maximum error for a reduction order by domain equal to 80.

Table 2
Test cases parameters.

Test case	h_{eq1} ($W m^{-2} K^{-1}$)	h_{eq2} ($W m^{-2} K^{-1}$)	T_{eq1} (°C)	T_{eq2} (°C)
1	1000	1000	20	40
2	10 000	10 000	20	40
3	40 000	40 000	20	40

Error comparison is made with the detailed model *A*. Two errors are computed:

- the maximum error

$$\epsilon_{max} = \max_t\left(\max_\Omega\left(\text{abs}(\widetilde{T} - T_A)\right)\right) \tag{31}$$

- the mean error

$$\epsilon_{mean} = \frac{1}{N_t V_\Omega}\sum_{i=1}^{N_t}\left(\int_\Omega \text{abs}(\widetilde{T} - T_A)\right) \tag{32}$$

3.4.1. Influence of parameter β for differents tests cases

Figs. 7 and 8 present the maximum error for a reduced model characterized by an order of reduction by domain $\widetilde{N} = 10$ and $\widetilde{N} = 80$, respectively, versus β, and for different amalgam test cases defined in Table 2. The first observation is that the flux jump penalization function has an important role: for an optimized β value, the reduced model results are clearly more precise than without this function (this case corresponds in the figure to the smallest value of β). However for β greater than the optimized value, the error becomes important there is so a compromise to find.

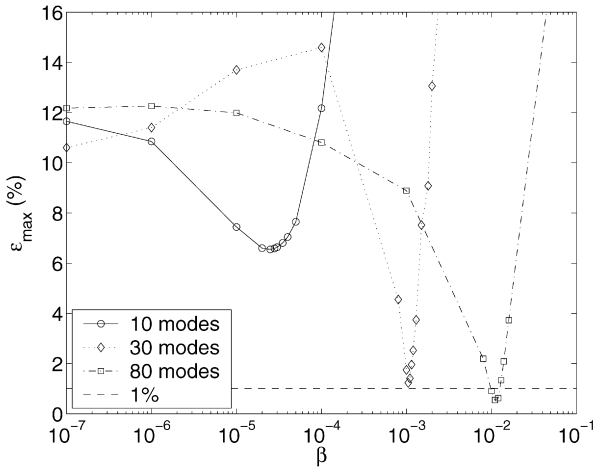

Fig. 9. Maximum error for an adaptated amalgam test cases (test case 1 in Table 2).

Concerning the amalgam reduction test case, the choice of the internal boundary condition (h_{eq1}, h_{eq2}, T_{eq1}, T_{eq2}) is quite large. As long as the choice is physically acceptable, the reduced model obtained from the test case is pertinent. In our application, the only non-adapted internal boundary corresponds to the extreme test case number 3. This condition is particularly unadapted for a reduced model characterized by an order of reduction by domain ($\widetilde{N} = 10$), and leads to important errors whatever the β value.

3.4.2. Influence of parameter β with the order of reduction

As explained above, for a reduced model a flux jump penalization function has to be added in order to optimize results. The flux jump is physically equal to zero, so there is not any physically justifiable choice for parameter β in Eq. (14). The problem is then to choose the β optimized value. A parametric study of β influence is made in this sense.

Fig. 9 compares the β influence on the maximum error for different reduced model orders. Without flux jump penalization ($\beta = 10^{-7}$) and for all the reduction orders, the maximum errors are close to each other and greater than 10%. With an optimized β value, results are clearly better, the more the order of reduction increases, the smaller the error is. For a small reduction order, the maximum error is already divided by two, and for an important reduction order the precision is improved by a factor 20. Furthermore the optimized β value dramatically depends on the reduction order, since between the two extreme cases (10 and 80 modes) the optimized β varies approximatively from 2×10^{-5} to 10^{-2}. That is why for a fixed value β (for example, 10^{-5}) the best precision corresponds to the reduction order $\widetilde{N} = 10$.

3.4.3. Blind choice of β

Comparison with the reference finite model *A* showed that there is an optimal trade-off for the β value. A method to determine this value without any knowledge of a reference solution is presented here.

For inverse problems using a Tikhonov regularization, the L-curve [15] provide an optimal choice for the trade-off on the penalization parameter value. In our case, the minimum of $\gamma(\beta)$ is close to the minimum of $\epsilon_{max}(\beta)$. $\gamma(\beta)$ is defined as:

$$\gamma(\beta) = \max_t\left(\frac{\|x^{n+1} - x^n\|_2}{\delta t^n}\right) \tag{33}$$

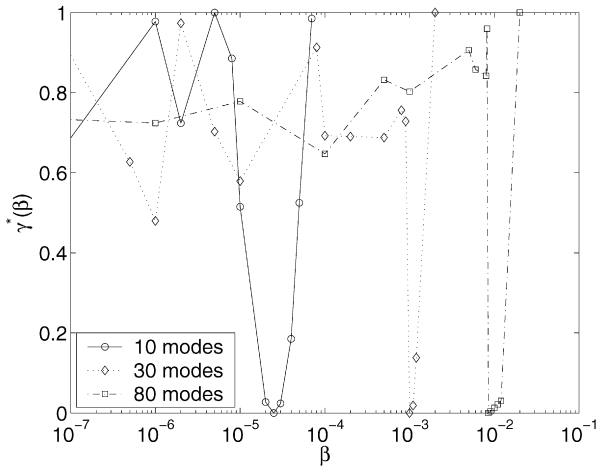

Fig. 10. Normalized $\gamma^*(\beta)$ (test case 1 in Table 2).

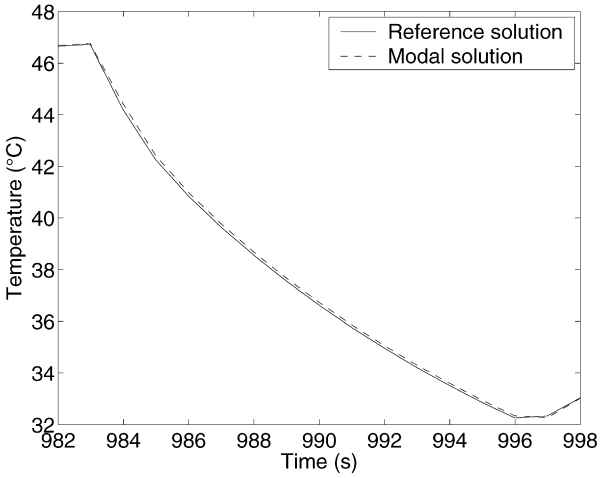

Fig. 11. Time evolution zoom for the point M where $\epsilon_{\max}(M)$ is maximum.

Table 3
Reduction results.

$\widetilde{N}$	10	30	80
ϵ_{mean} (°C)	0.1087	0.04880	0.01930
$\epsilon_{\max}$ (°C)	2.387	0.5144	0.199
Computation time (s)	24	43	199

Where x^n denotes the state vector at the iteration number n and δt^n the time increment at this iteration, the simulation is done with the corresponding β.

For a graphical convenience we plot in Fig. 10 the normalized $\gamma^*(\beta)$:

$$\gamma^*(\beta) = \frac{\gamma(\beta) - \min_\beta(\gamma(\beta))}{\max_\beta(\gamma(\beta)) - \min_\beta(\gamma(\beta))} \tag{34}$$

3.4.4. Computation time

Table 3 presents the computation time needed for simulation in modal space and temperature field reconstruction. The modal basis determination is not included. β influence on computation time is negligible: in the case of $\widetilde{N} = 80$, computation time is equal to 199 ± 1 s.

With a reduction order equal to 80, the reduced model provides the same precision than the detailed model B, but with a computation time gain equal to 82.

3.4.5. Error

With a reduction order equal to 80, informations on the entire temperature field (in time and in space) is computed with an maximum error ($\epsilon_{\max}$) less than 0.2 K for the whole simulation. Fig. 11 presents a time evolution zoom at the point M where $\epsilon_{\max}(M)$ is maximum (so $\epsilon_{\max}(M) = \epsilon_{\max}$):

$$\epsilon_{\max}(M) = \max_t\left(\text{abs}\left(\widetilde{T}(M) - T_A(M)\right)\right) \tag{35}$$

The control process imposing the extreme temperatures, the error linked to the reduce model induces a temporal drift. Physically there is a drift in the fan speed switch. That is why the error between both models corresponds to the temporal drift equal to 0.2 s comparing to cycle period equal to 106 s.

4. Conclusion

This work presented results of the substructuring technique adapted to the branch modal reduced models. This technique allows to extend the application domain of branch reduced models, since it becomes possible to solve a non-linear thermal problem with a thermal contact resistance. Three points can be underlined:

- The reduction method used here corresponds to the amalgam method developed initially for a non-substructuring problem, in which an unique branch basis is obtained for the whole considered domain. The choice of the test cases necessary for this method is not obvious, because a test case has to be found for each subdomain considered as independent. These test cases do not then correspond to the real problem. However, the test cases choice is not sensitive on the reduced model precision, and good results are obtained for a wide range of parameters.
- This method gives better results when a flux jump penalization is added to the state equation. Studies showed that the ponderation coefficient β of the flux jump penalization has a very important effect. For an reduction order of 80, the precision is 20 times better with an optimal penalization than without. However an unadapted β value could reduce precision of the results in comparison with unpenalized ones. The penalization level is a function of the flux error, explaining why the optimal β value is a function of the reduction order. The β value choice is possible with the graphical study of $\gamma(\beta)$.
- This study proves the efficiency of the proposed method. In the case of the studied electronic component, a precision equivalent to the detailed discrete problem is obtained with a gain in computation time equal to 82.

References

[1] http://www.caam.rice.edu/software/ARPACK/.
[2] A. Baeza, A. Roda, J.C.O. Nielsen, Railway vehicle/track interaction analysis using a modal substructuring approach, J. Sound Vib. 293 (2006) 112–124.
[3] R.A. Białecki, A.J. Kassab, A. Fic, Proper orthogonal decomposition and modal analysis for acceleration of transient FEM thermal analysis, Int. J. Numer. Meth. Eng. 62 (2005) 774–797.
[4] F. Brezzi, B. Cockburn, L.D. Marini, E. Süli, Stabilization mechanisms in discontinuous Galerkin finite element methods, Comput. Method. Appl. Mech. 195 (2006) 3293–3310.
[5] M. Broussely, Y. Bertin, P. Lagonotte, Reduction and optimisation of thermal models using Kirchhoff network theory, Int. J. Therm. Sci. 42 (2003) 795–804.
[6] A. El Biyaali, J.J. Roux, C. Inard, Sous-structuration et couplage de modèles réduits appliqués aux transferts thermiques dans le sol, Int. Commun. Heat Mass 3 (1996) 575–586.
[7] B. Flament, F. Bourquin, A. Neveu, Synthèse modale : une méthode de sous-structuration dynamique pour la modélisation des systèmes thermiques linéaires, Int. J. Heat Mass Tran. 36 (1993) 1649–1662.
[8] J.P. Gwinn, R.L. Webb, Performance and testing of thermal interface materials, Microelectron. J. 34 (2003) 215–222.
[9] F. Hirsch, G. Lacombe, Elements of Functional Analysis, Graduate Text in Mathematics, vol. 192, Springer, Berlin, 1999.
[10] S.A. Marshall, An approximate method for reducing the order of a linear system, Control (1966) 642–653.

[11] A. Ménézo, J.J. Roux, J. Virgone, Modelling heat transfers in building by coupling reduced-order models, Build. Environ. 37 (2002) 133–144.
[12] A. Neveu, K. El Khoury, B. Flament, Simulation de la conduction non linéaire en régime variable : décomposition sur les modes de branches, Int. J. Therm. Sci. 38 (1999) 289–304.
[13] A. Oulefki, A. Neveu, Réduction par amalgame modal d'un modèle thermique, J. Phys. III (2) (1993) 303–320.
[14] O. Quéméner, A. Neveu, E. Videcoq, A specific reduction method for the branch modal formulation: Application to a highly non-linear configuration, Int. J. Therm. Sci. 46 (2007) 890–907.
[15] N. Renault, S. André, D. Maillet, C. Cunat, A two-step regularized inverse solution for 2-D heat source reconstruction, Int. J. Therm. Sci. 47 (2008) 834–847.
[16] D. Ryckelynck, A priori hyperreduction method: an adaptative approach, J. Comput. Phys. 202 (2005) 346–366.
[17] J.J. Salgon, A. Neveu, Application of modal analysis to modelling of thermal bridge in buildings, Energ. Buildings 10 (1987) 109–120.
[18] T. Shih, J.T. Skladany, An eigenvalue method for solving transient heat conduction problems, Numer. Heat. Transfer 6 (1983) 409–422.
[19] D.C. Sorensen, Implicitly Restarted Arnoldi/Lanczos Methods for Large Scale Eigenvalue Calculations, Kluwer, 1995, pp. 23–25.